RSC Advances

Chemical Synthesis of PANI-TiO2 Composite Thin Film for Supercapacitor Application

Journal:	*RSC Advances*
Manuscript ID:	RA-ART-05-2015-009233.R2
Article Type:	Paper
Date Submitted by the Author:	22-Jul-2015
Complete List of Authors:	Deshmukh, Prashant; Shivaji University Kolhapur, Physics Patil, Sandip; Shivaji University Kolhapur, Physics Bulakhe, Ravindra; Shivaji University, Physics Pusawale, Swati; Shivaji University, Kolhapur, Department of Physics Shim, Jae-Jin; Yeungnam University, School of Chemical Engineering Lokhande, Chandrakant; Shivaji University, Physics

Chemical Synthesis of PANI-TiO_2 Composite Thin Film for Supercapacitor Application

P. R. Deshmukh[a,b], S. V. Patil[a], R. N Bulakhe[a,b] , S. N. Pusawale[a], J. J. Shim[b] and C. D. Lokhande[a]*

[a]Thin Film Physics Laboratory, Department of Physics, Shivaji University, Kolhapur- 416 004 (M. S.) India.

[b]Supercritical Fluids and Nanoprocess Laboratory, School of Chemical Engineering, Yuengnam University, South Korea, 712-749.

Abstract

A unique and cost effective chemical route has been carried out for the synthesis of Polyaniline-Titanium oxide (PANI-TiO_2) composite thin film at room temperature. Characterization techniques, such as Fourier transform infrared and FT-Raman spectroscopy; have shown the formation of composite. The result of X-ray diffraction indicates the amorphous nature of PANI-TiO_2 composite thin films. The morphology of PANI-TiO_2 composite thin film observed using scanning electron microscope shows porous framework of agglomerated nanofibers. The electrochemical characterization of the pseudocapacitive PANI-TiO_2 composite in 1 M H_2SO_4 electrolyte displayed highest specific capacitance of 783 $F.g^{-1}$ at the scan rate of 5 $mV.s^{-1}$. The synergistic effect between PANI with its counterpart TiO_2 caused an increased cycle stability of 78% over 5000 consecutive cycles, which is higher than the virgin PANI with 70% specific capacitance retention. The distinctive structure of PANI-TiO_2 composite and the cohabitation of conducting PANI with TiO_2 have found to be responsible for the superior electrochemical properties.

Keywords: Chemical Method, Composite, Thin Film, Supercapacitor.

*Corresponding Author: Prof. C. D. Lokhande, E-mail: l_chandrakant@yahoo.com

Tel.: +91 231 2609225, Fax: +91 231 2692333.

1 Introduction

Supercapacitors an intermediate power and energy source between dielectric capacitors and batteries have emerged as an important energy storage technology due to high power delivery, high cycle stability and long life time. Supercapacitors have found various applications in memory backup, hybrid electric vehicles, medical, military, aerial lift, public transport buses, uninterruptible power sources in banking centers, hospitals, airport control towers, cell phone towers, etc. Supercapacitor, an ecofriendly energy resource, has minimized the limitations of the other two conventional energy sources, the rechargeable battery and the capacitor, in terms of both high power density and high energy density **[1-3].**

On the basis of charge storage mechanism as well as active materials of electrodes, supercapacitor can be divided into two categories. One is the electrochemical double layer

capacitors (EDLCs), which stores energy by forming a double layer of electrolyte ions on the surface of conductive electrode, and the most common devices are carbon based active materials with high specific surface area at present. The other is the pseudocapacitors, whose capacitance arises from Faradaic reactions at the surface of active materials. Transition metal oxides and electrically conducting polymers are extensively studied as pseudocapacitive active materials **[4, 5]**. Among the various conducting polymers, polyaniline (PANI) is considered as a most promising material because of its high capacitive characteristic, low cost, and facile synthesis **[6].** However, the poor stability during the charge-discharge process restricts its practical application in supercapacitor. One of the ways to improve the performance of PANI based supercapacitors in terms of stability is to combine PANI with transition metal oxide materials. Transition metal oxides, such as RuO_2, MnO_2, V_2O_5, and SnO_2, contribute pseudocapacitance as well as enhance the stability of composite materials **[7-10]**. Polymer-metal oxides composite electrode shows the enhanced supercapacitive properties than the pristine electrode material. For example; PANI and metal oxides composite have been demonstrated to strengthen not only the improved capacitance value but also cyclic stability of PANI. Here the counter part inorganic/metal oxide electrodes, constrain the change in volume of PANI as well as provide the larger surface as as well as shorter ion path for electrodes **[11]**. However, these transition metal oxides suffer from low abundance, a high cost for their raw materials, low electrical conductivity. Therefore, alternative to these transition metal oxides, researchers have considered TiO_2 as a promising transition metal oxide material for polymer composite supercapacitor, due to its high specific energy density, low cost, nontoxicity, ecofriendliness, and abundant availability **[12]**. Xu et al. obtained the maximum specific capacitance of 335 $F.g^{-1}$ for the ternary composite of PANI/neutral red/TiO_2 (PANI/PNR/TiO_2) prepared by chemical oxidation polymerization **[13]**. Bian et al. reported maximum specific capacitance of 330 $F.g^{-1}$ for fibriform PANI-TiO_2 composite synthesized by one step in situ polymerization of aniline in the presence of TiO_2 particles **[14]**.

Here, we have developed chemical route for the synthesis of PANI-TiO_2 composite thin film. The synthesis method we used here is simple in comparison with other methods, and has a great potential for the commercialization of the technology. PANI-TiO_2 composite thin film was successfully prepared by in-situ polymerization of aniline in the presence of TiO_2 nanoparticles. The supercapacitive performance of PANI-TiO_2 composite thin film electrode evaluated with cyclic voltammetry, galvanostatic charge-discharge and electrochemical impedance spectroscopy study. The stability of the PANI-TiO_2 composite thin film electrode was studied, in order to check the life cycle of electrode material. The

comparative study of supercapacitive properties of PANI and PANI-TiO_2 composite thin film electrode has been made.

2 Experimental Details

2.1 Synthesis of PANI

The synthesis of PANI thin film was carried out by chemical polymerization of aniline monomer at room temperature. During the synthesis, the solution was prepared with 0.2 M aniline monomer dissolved in 1 M H_2SO_4 and an oxidizing agent of 0.1 M ammonium persulfate. The stainless steel substrates were placed in the solution. When the polymerization starts in solution, heterogeneous reaction occurs and the growth of PANI observed on the substrate. The thin PANI coating of 0.013 $mg.cm^{-2}$ thickness was observed after 30 minute of polymerization. The optimum time for the maximum growth of PANI on the stainless steel substrate was 30 minute, after that no growth of PANI on the substrate was observed. The thickness obtained was not sufficient for the supercapacitive study. Therefore, in order to increase the film thickness we have repeated the same process for four times. However, the terminal thickness of 0.13 $mg.cm^{-2}$ was obtained at third deposition. For further deposition, decrease in film thickness observed, which could be attributed to the formation of outer porous layer and/or the film which may develop stress to cause delamination, resulting in peeling off the film after the film reaches at maximum thickness **[15, 16].**

2.2 Experimental Setup for Deposition of PANI-TiO_2 Composite Thin Films

Aniline, $TiCl_3$ and ammonium persulphate solution were used as the starting materials to synthesize PANI-TiO_2 composite thin films. The procedure carried out was as follows: A solution of 0.02 M $TiCl_3$ was aged for 5 days to make a sol of TiO_2. Initial day, the color of the solution is transparent violet color. As the day's passes, the color of the solution starts to change from transparent violet to whitish. After the fourth day, it completely turned into whitish color sol and there was formation of TiO_2 powder on the six day. The TiO_2 sol was then treated with a solution of 0.1 M aniline and 1 M H_2SO_4 with optimized volume ratio 1:1. The clean and mirror polished stainless steel substrates were vertically immersed in the bath. Then 0.1 M ammonium persulphate as an oxidant was added to the homogeneous mixture of aniline and TiO_2 sol. The color of the solution gradually changed to blue, dark blue and finally dark green, indicating the polymerization of aniline in the solution. After 30 minute the precipitation starts to settle down in the beaker. The maximum thickness obtained was 0.03 $mg.cm^{-2}$ on the stainless steel substrate. In order to increase the film thickness, repeated depositions were carried out using the same compositional bath. The maximum thickness was observed after the third deposition, and afterwards thickness was decreased.

2.3 Characterization Techniques

The X-ray diffraction (XRD) analysis was carried out using diffractometer with chromium target of wavelength 2.29 Å. Surface morphology was studied with the help of scanning electron microscope (SEM) model JEOL–JSM 6360. Fourier transform infrared (FT-IR) spectroscopy was recorded between 4000-400 cm^{-1} at a spectral resolution of 2 cm^{-1} on a PerkinElmer 1710 spectrophotometer using KBr pellets at room temperature. The FT-Raman spectroscopy study conducted using Bruker made FT-Raman spectrophotometer. Samples in the powder form were excited with a 514.5 nm Argon laser (0.5 mW), using a Perkin-Elmer, model 783, USA. The cyclic voltammetry (CV) study was carried out using the 263A EG & G Princeton Applied Research Potentiostat forming an electrochemical cell consisting of PANI-TiO_2 composite electrode as working electrode, platinum as a counter electrode and saturated calomel electrode (SCE) as a reference electrode. The dipped area of the working electrode stainless steel substrate in the electrolyte and size of platinum counter electrode was 1 cm^2. The WonATech Automatic Battery Cycler WBCS3000 system used to study the charge-discharge of PANI-TiO_2 composite electrode. The electrochemical impedance measurement conducted with WonATech made electrochemical workstation (ZIVE SP5).

3 Results and Discussion

3.1 PANI Thin Film Formation and Reaction Mechanism

PANI is composed of aniline repeat units connected to form a backbone. An efficient polymerization of aniline is achieved only in an acidic medium, where aniline exists as an anilinium cation. The oxidation of monomers forms a radical cations followed by coupling to form di-cations and its repetition leads to the polymer formation. The oxidation process is accompanied by the insertion of anions of acid solution in order to maintain the charge neutrality of the PANI. In this case, hydrogen atoms preoccupied from aniline molecules during their blending to oligomeric and polymeric structures released as protons, i.e. sulfuric acid as a by product. The oxidation of aniline with ammonium persulphate (APS) to yield PANI and other by products is presented in scheme 1 **[17, 18]**,

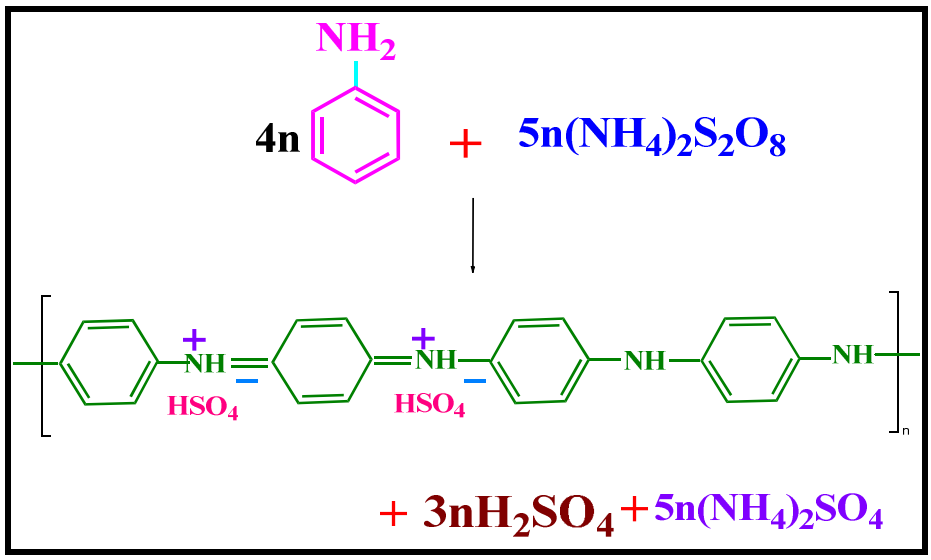

Scheme 1: Aniline oxidized with ammonium persulphate to form PANI, Sulfuric acid and ammonium sulphate are by products.

3.2 PANI-TiO_2 composite Thin Film Formation and Reaction Mechanism

Fig. 1A shows the schematic representation of chemical route for the deposition of PANI-TiO_2 composite thin film. Preparation of PANI-TiO_2 composite thin film is based on the polymerization of aniline monomer and attaching of TiO_2 particle to PANI during formation. The actual experimental set up for the formation of PANI-TiO_2 composite thin film is shown in **Fig. 1B** and it is explained in the following way: The 0.02 M $TiCl_3$ was aged for five days. The color of the solution changes from transparent violet solution to whitish, as the day increases **(Fig. 1B)**. This solution was used for the deposition of PANI-TiO_2 composite. The equal volume of an aniline monomer and the aged TiO_2 solution **(Fig. 1A (a and b))** was taken in bath. In this chemical bath, 0.1 M ammonium persulphate oxidant was added for the polymerization of aniline **(Fig. 1A (c)).** Within few minutes, the color of the bath turns from whitish to dark green indicating the polymerization of aniline. As the reaction proceeds, the TiO_2 particles attaches to the surface of PANI globular particles, finally depositing a thin layer on the substrates. It leads to an adhesion of the PANI to TiO_2 particles on the substrate **[19, 20].** Because titanium is a transition metal and has intense tendency to form the coordination compound with nitrogen atom in PANI molecular, such adhesion will not only constrain the motion of PANI chains, but also restricts the vibration mode in PANI **[21].** This deposition process was repeated for 3 times to obtain the maximum thickness. The film thickness was found to be increased with number of depositions and remained constant after third deposition. The obtained maximum thickness of PANI-TiO_2 composite is 0.18 $mg.cm^{-2}$ on the stainless steel substrate.

Rotzinger **[22]** and Gratzel **[23]** have reported on the kinetics of decomposition of $TiCl_3$ solution. Reaction of Ti (III) with O_2 is rate determining step in TiO_2 formation. The $TiOH^{2+}$ is the only reactive species as per the reactions represented below,

$$Ti^{3+} + H_2O \rightarrow TiOH^{2+} + H^{+} \quad 2$$

$$TiOH^{2+} + O_2 \rightarrow TiO_2 + 2OH^{-} \quad 3$$

The reaction mechanism of PANI-TiO_2 composite formation is schematically shown in **Fig. 2A.** The photographs of (a) PANI and (b) PANI-TiO_2 composite thin films on the stainless steel substrate are shown in **Fig. 2B.** Here, the PANI thin film color is dark green, while the green color of PANI film slightly changed to whitish green for PANI-TiO_2 composite thin film showing the the presence of TiO_2. The large deposition area (> 10 cm^2) indicates that, this method is feasible for the large area deposition of thin film as well as composites of polymer and metal oxide.

3.3 X-ray Diffraction Study

The XRD patterns of (a) PANI and (b) PANI-TiO_2 composite films onto the stainless steel substrate are shown in **Fig 3**. All the XRD patterns consist of no well defined diffraction peaks other than stainless steel substrate, indicating that synthesized thin films are amorphous in nature. Here, only the stainless steel peaks are present in the PANI and PANI-TiO_2 composite thin film XRD patterns. However, in this case, the material may be formed in the form nano crystalline form, but because of more intense peaks of stainless steel; we cannot find the peaks corresponding to TiO_2 or PANI thin films. But the presence of TiO_2 and PANI-TiO_2 composite material is confirmed from FT-IR and FT Raman spectroscopy, which are more sensitive to identify to the presence of bonding or stretching vibrations in the synthesized TiO_2 and PANI-TiO_2 composite. The amorphous phase is feasible for supercapacitor application, since the protons can easily permeate through the bulk of the amorphous material electrode and whole amount of electrode is utilized for energy storage **[24, 25]**.

3.4 Surface Morphological Study

The morphology of PANI and PANI-TiO_2 composite thin films was studied using scanning electron microscopy. **Fig. 4 (a) and (b)** shows the SEM images of PANI and PANI-TiO_2 composite thin films on the stainless steel substrate at x 10,000 magnification. PANI SEM shows full coverage of the substrate by stacked globular structure. The porous framework of agglomerated nanofibers arranged on the substrate surface observed for PANI-TiO_2 composite thin film. The average diameter of nanofiber observed to be ~ 20-50 nm. The globular structure of PANI has been changed to agglomerated nanofibers in the PANI-TiO_2

composite. This leads to an indication of strong interaction between TiO_2 particle, which may interrupt secondary reaction of PANI and continues in the nanofiber formation.

3.5 Fourier Transform Infrared (FT-IR) and FT-Raman Spectroscopy Study

Fig. 5A shows the FT-IR spectra of (a) PANI and (b) PANI-TiO_2 composite thin films in the range of 4000–450 cm^{-1}. **Fig. 5 (A-a)** shows the FT-IR spectrum of PANI thin film. The characteristic peaks of PANI were assigned as follows: the band at 3408 cm^{-1} is attributable to N–H stretching mode, the band at 2901 cm^{-1} is assigned to vibration associated with the NH^{2+} part in the $–C_6H_4NH^{2+}C_6H_4$- group, the peaks at 1603 cm^{-1} is attributable to C=N for the quinoid and 1461 cm^{-1} is C=C stretching mode for benzenoid rings; the peak at 1110 cm^{-1} was formed during protonation, and can be assigned to in-plane bending vibration of C-H, the peak at 1019 cm^{-1} can be attributable to out of plane bending vibration of C-H **[7, 26].**

All the characteristic peaks of PANI observed in the PANI-TiO_2 composite spectrum are shown in **Fig. 5 (A-b).** The peaks in the composite corresponding to PANI have been shifted as compared with PANI as follows: the peak at 2901 cm^{-1} is shifted to 2931 cm^{-1} which is attributed to the NH^{2+} part in the $–C_6H_4NH^{2+}C_6H_4$- group, the peak at 1603 cm^{-1} is shifted to 1573 cm^{-1} which is assigned to the C=N for the quinoid, the peak at 1461 cm^{-1} shifted to 1477 cm^{-1} which is assigned to the C=C stretching mode for benzenoid rings. The main characteristic peaks of PANI at 1573 cm^{-1} (C=C stretching mode for the quinonoid unit), 1477 cm^{-1} (C=C stretching mode for benzenoid unit), 1301 cm^{-1} (C–N stretching mode of benzenoid unit), 1109 cm^{-1} (N=Q=N, where Q represents the quinonoid unit), 810 cm^{-1} (out-of-plane C-H bending mode) appeared in the FT-IR spectrum of the PANI-TiO_2 composite thin film. The main absorption peak of pure TiO_2 assigned Ti-O-Ti bond appear at 601 cm^{-1} **[27, 28].** In **Fig. 5 A**, the peaks of the composites are shifted to higher wavenumbers due to the strong interaction that exists at the interface of PANI and TiO_2 nanoparticles **[29].**

The FT Raman spectroscopy technique is sensitive to the electronic structure and vibrational properties of conducting polymers as well as metal oxide. **Fig. 5 B** shows the FT-Raman spectra of (a) PANI and (b) PANI-TiO_2 composite thin films. From both FT-Raman spectra, it can be clearly seen that FT-Raman spectrum of the PANI-TiO_2 composite is different from that of PANI. **Fig. 5 (B-a)** shows a typical FT-Raman spectrum of PANI thin film prepared by chemical route. In this Raman spectrum, the C-H bending of the quinoid ring at 1170 cm^{-1}, C-N^+ stretching at 1372 cm^{-1}, and C-C stretching of the benzene ring at 1506 and 1597 cm^{-1} reveal the presence of the doped PANI-ES (Emeraldine Salt) structure **[30, 31].** In the FT-Raman spectrum of PANI, the peaks at 1594 and 1170 cm^{-1} have been attributed to the benzenoid units, while the peak at 1372 cm^{-1} is due to the quinonoid units.

However, a new band (1507 cm^{-1}) appeared in PANI-TiO_2 composite, and the intensity of bands at 1171 and 1594 cm^{-1} is strengthened obviously. Moreover, the characteristic peaks of TiO_2 disappeared in the composite. These results indicate that PANI and TiO_2 nanoparticles not only simply blended or mixed up but also they exists strong interaction at the interface of PANI and TiO_2. Here, it is observed that PANI probably encapsulates TiO_2 nanoparticles or TiO_2 nanoparticles are entrapped in PANI chains **[32].**

3.6 Electrochemical Properties

The CV curves of PANI and PANI-TiO_2 composite electrodes were performed in the potential window -0.2 to +0.8 V vs SCE at the scan rate of 5 $mV.s^{-1}$ and are shown in **Fig. 6 A.** From **Fig. 6 A,** it is seen that PANI and PANI-TiO_2 composite electrode shows redox processes, which are related to the typical interconversion reaction of PANI upon varying the potential. The area under curve for PANI-TiO_2 composite is greater than the PANI electrode. The capacitance 'C' of composite thin film electrode was calculated from the relation **[33]**,

$$C = \frac{I}{(dv/dt)} \quad (4)$$

Where, 'I' is the average current in amperes and (dv/dt) is the scan rate in V/s. Similarly the interfacial capacitance (C_i) is obtained by dividing the capacitance (C) by respective electrode area in the electrolyte as follows:

$$C_i = \frac{C}{A} \quad (5)$$

Where 'A' is the area (1 cm^2 in this study) of electrode dipped in the electrolyte. The specific capacitance (C_s) of the electrode is obtained by dividing the capacitance (C) by the weight of PANI-TiO_2 composite thin film electrode as follows:

$$C_s = \frac{C}{W} \quad (6)$$

Where 'W' is the weight of the PANI-TiO_2 composite thin film electrode dipped in the electrolyte **[3]**.

The CV curves of PANI-TiO_2 composite electrode at different scan rates are shown in **Fig. 6 B**. The proton transfer process is slow at higher scan rate therefore it leads to either depletion or saturation of the protons in the electrolyte inside the electrode during the redox process. This mainly results in the increase of ionic resistivity leading to the drop in the capacitances of the electrode. **Fig. 6 C and D** show the variation of specific and interfacial capacitances with scan rate of the (a) PANI and (b) PANI-TiO_2 composite thin film electrodes. The decreasing trend of the capacitance suggests that parts of the surface of the

electrode material are inaccessible at higher scan rates. Hence, the specific capacitance obtained at the slow scan rates is believed to be closest to that of full utilization of the electrode material. At lowest scan rate of 5 $mV.s^{-1}$, maximum specific capacitance is found to be 591 and 783 $F.g^{-1}$ for PANI and PANI-TiO_2 composite electrodes, respectively. **Table 1** gives the summary of PANI–TiO_2 composite thin film based supercapacitor with their key performance features. For the better comparative study with the literature, the specific capacitance was calculated using the using the equation 7. The obtained specific capacitance in this study is larger than the reported specific capacitance values of PANI-TiO_2 composite synthesized by chemical polymerization in the literature **[11, 13, 14, 34]**. From the **Fig. 6 C and D,** it is observed that the specific as well as interfacial capacitance of PANI and PANI-TiO_2 composite electrode decreases as the scan rate increases.

Fig. 7 shows the specific capacitance of (a) PANI and (b) PANI-TiO_2 composite as a function of cycle number for 5000^{th} cycles. It is observed that the initial decay of the specific capacitance of the PANI electrode is more than the PANI-TiO_2 composite electrode upto 1500 cycles. After that, there is small decay in the specific capacitance of the PANI and PANI-TiO_2 composite electrodes. Inset of figure shows the cyclic voltammetric curves of PANI-TiO_2 at the scan rate of 100 $mV.s^{-1}$ for the 1^{st} and $5{,}000^{th}$ cycles. The current density of PANI-TiO_2 electrode decreased upto 78% within $5{,}000^{th}$ cycles. The PANI-TiO_2 composite electrode shows better stability than the PANI electrode for 5000^{th} CV cycles. Here, TiO_2 nanoparticles may provide shield to volume change of PANI during stability, because of counter ions intercalation/deintercalation. In addition, this may prevent the breakage of PANI chain during the charging and discharging process resulting stable chain structure. Therefore, synergestic effect of TiO_2 combined with the conducting PANI plays an important role not only in decreasing mechanical degradation but also for diffusion of the electrolyte ions sufficiently. This results in more available surface area for effective utilization to deliver a high specific capacitance. Hence one can say that the TiO_2 enhances the stability of PANI electrode in PANI-TiO_2 composite electrode **[35, 36]**.

Fig. 8 A shows the galvanostatic charge-discharge curves of (a) PANI and (b) PANI-TiO_2 composite thin films carried out with constant current density of 0.5 $mA.cm^{-2}$ in the potential range of -0.2 to +0.8 V vs. SCE. As shown in **Fig. 8 A,** the curves are not ideal straight lines indicating the process of a faradic reaction. On the other hand, there was an initial potential drop caused by internal resistance, which arises from the resistance of both the electrolyte and the electrode material **[37].** The specific capacitance (C_s, $F.g^{-1}$), specific energy (SE, $Wh.kg^{-1}$), and the specific power (SP, $kW.kg^{-1}$) calculated from the charge-discharge curve using the following equations (7-9), respectively **[3, 36, 38,]**:

$$C_s = \frac{I \times \Delta t}{m \times \Delta V} \quad (7)$$

$$SE = \frac{1}{2} C_s V^2 \quad (8)$$

$$SP = \frac{SE}{\Delta t} \quad (9)$$

Where, C_s ($F.g^{-1}$) is the capacitance, I (A) shows the discharge current, ΔV (V) is the potential change within the discharge time Δt (s), m (g) is the weight of the active material. The columbic efficiency is calculated using the following equation **[3, 15]:**

$$\eta = [\frac{t_D}{t_C}] \times 100 \quad (10)$$

Where, t_C and t_D represent the time of charging and discharging, respectively. The specific power, specific energy and columbic efficiency are shown in **Table 2.** The PANI-TiO_2 electrode materials responded in a wide range of working potentials of −0.2 V to +0.8 V, which indeed resulted in a high energy density without substantial loss of power density. The highest power density of 1.83 $kW.kg^{-1}$ corresponds to 391.5 $Wh.kg^{-1}$ energy density of PANI-TiO_2 composite thin film electrode. From the table 2 it is observed that the PANI-TiO_2 composite electrode shows better supercapacitor properties than the pristine PANI electrode. The conducting polymer composites exhibit good charge-discharge properties, indicating clearly that the conducting polymer can work as a conducting matrix for the TiO_2 particles.

Impedance spectroscopy is a powerful method of evaluating a components performance in the frequency domain. **Fig. 8 B** shows Nyquist plots of (a) PANI and (b) PANI-TiO_2 composite thin film electodes. Common features observed in the Nyquist impedance plots of PANI and PANI-TiO_2 composite electrodes are semicircles at high frequencies and lines at medium to low frequencies. The semicircles correspond to the bulk film resistance in parallel with the geometric capacitance and/or to interfacial charge transfer **[39].** The lines observed at the middle and low frequencies are due to the charge transport impedance that originates from non uniform concentration profiles of charged species in the film **[12]**. Inset of **Fig. 8 B** shows the expanded view of semicircles of PANI and PANI-TiO_2 electrode. The Electrochemical charge transfer resisitance values observed for PANI and PANI-TiO_2 composite electrodes are 27 and 20 Ω, respectively.

4. Conclusions

The PANI-TiO_2 composite thin films have been synthesized using simple chemical route. The XRD study revealed amphorphous nature of the PANI-TiO_2 composite thin film.

The well dispersed agglomerated network of PANI-TiO_2 nanofibers on the stainless steel substrate is observed from the surface morphology of PANI-TiO_2 composite thin film. The presence of elemental bonding has confirmed from the FT-IR and FT-Raman spectra and the little shift of characteristics peaks of PANI in the PANI-TiO_2 spectrum show the formation of composite material. The PANI-TiO_2 composite electrode shows the maximum specific capacitance of 783 $F.g^{-1}$ at the scan rate of 5 $mV.s^{1}$, which is greater than the PANI (591 $F.g^{-1}$). Comparative study of PANI and PANI-TiO_2 composite shows an enhanced stability of PANI electrode after the composite formation with TiO_2. The stability of the PANI-TiO_2 composite electrode showed 78% over the 5000^{th} cycles. The specific power, specific energy and columbic efficiency have found to be 1.83 $kW.kg^{-1}$, 391.5 $Wh.kg^{-1}$ and 96 %, respectively. The EIS study showed that the PANI and PANI-TiO_2 composite electrode are more suitable for use at a low frequency region.

Acknowledgment

Authors are grateful to UGC and DST New Delhi, India for providing finance through the UGC-DSA-Phase-I, DST-PURSE and DST-FIST programme to the Department of physics, Shivaji University Kolhapur-India. Also, this research is supported by the Priority Research Centers Program through the National Research Foundation of Korea (NRF) funded by the Ministry of Education (2014R1A6A1031189).

References

[1] D. Ghosh, S. Giri, Md. Moniruzzaman, T. Basu, M. Mandal, C. K. Das, Dalton Trans., 43 (2014) 11067.

[2] P. A. Basnayaka, M. K. Ram, L. Stefanakos, A. Kumar, Graphene, 2 (2013) 81.

[3] P. R. Deshmukh, N. M. Shinde, S. V. Patil, R. N. Bulakhe, C. D. Lokhande, Chem. Engg. J., 223 (2013) 572.

[4] C. D. Lokhande, D. P. Dubal, O. S. Joo, Curr. Appl. Phy. 11 (2011) 255.

[5] Y. Li, X. Zhao, Q. Xu, Q. Zhang, D. Chen, Langmuir, 27 (2011) 6458.

[6] T. C. Girija, M. V. Sangaranarayanan, J. Power Sources, 159 (2006) 1519.

[7] P. R. Deshmukh, S. V. Patil, R. N. Bulakhe, S. D. Sartaleb, C. D. Lokhande, Chem. Engg. J., 257 (2014) 82.

[8] F. Meng, X. Yan, Y. Zhu, P. Si, Nanoscale Res. Lett. 8 (2013) 179.

[9] M. H. Bai, T. Y. Liu, F. Luan, Y. Li, X. X. Liu, J. Mater. Chem. A, 2 (2014) 10882.

[10] Z. A. Hu, Y. L. Xie, Y. X. Wang, L. P. Mo, Y. Y. Yang, Z. Y. Zhang, Mater. Chem. Phy., 114 (2009) 990.

[11] S. Xie, M. Gan, L. Ma, Z. Li, J. Yan, H. Yin, X. Shen, F. Xu, J. Zheng, J. Zhang, J. Hu, Electrochim. Acta, 120 (2014) 408.

[12] A. Ramadoss, S. J. Kim, Carbon, 63 (2013) 434.

[13] H. Xu, Q. Cao, X. Wang, W. Li, X. Li, H. Deng, Mater. Sci. Engg., B 171 (2010) 104.

[14] C. Bian, A. Yu, H. Wu, Electrochem. Comm., 11 (2009) 266.

[15] P. R. Deshmukh, S. N. Pusawale, R. N. Bulakhe, C. D. Lokhande, Bull. Mater. Sci., 36 (2013) 1171.

[16] U. M. Patil, S. B. Kulkarni, P. R. Deshmukh, R. R. Salunkhe, C. D. Lokhande, J. Alloys Comp., 509 (2011) 6196.

[17] I. Sapurina, J. Stejskal, Polym. Intern. 57 (2008) 1295.

[18] P. R. Deshmukh, S. N. Pusawale, N. M. Shinde, C. D. Lokhande, J. Korean Phys. Soc., 64 (2014) 60.

[19] H. Xia, Q. Wang, Chem. Mater., 14 (2002) 2158.

[20] X . Li, G. Wang, X. Li, D. Lu, Appl. Surf. Sci., 229 (2004) 395.

[21] P. R. Somani, R. Marimuthu, U. P. Mulik, S. R. Sainkar, D. P. Amalnerkar, Synth. Met., 106 (1999) 45.

[22] F. P. Rotzinger, M. Grätzel, Inorganic Chem., 26 (1987) 3704.

[23] M. Grätzel, J. Sol-Gel Sci. Techn., 22 (2001) 7.

[24] A. Devadas, S. Baranton, T. W. Napporn, C. Coutanceau, J. Power Sources, 196 (2011) 4044.

[25] V. D. Patake, C. D. Lokhande, Appl. Surf. Sci., 254 (2008) 2820.

[26] S. B. Kulkarni, S. S. Joshi, C. D. Lokhande, Chem. Engg. J., 166 (2011) 1179.

[27] J. Mink, J. Kristof, A. D. Battisti, S. Daolio, C. Nemeth, Surf. Sci., 335 (1995) 252

[28] L. J. Zhang, M. X. Wan, J. Phys. Chem., B 107 (2003) 6748.

[29] X. B. Yan, Z. J. Han, Y. Yang, B. K. Tay, Sens. Actuat. B, 123 (2007) 107.

[30] G. Louarn, M. Lapkowski, S. Quillard, A. Pron, J. P. Buisson, S. Lefrant, J. Phys. Chem., 100 (1996) 6998.

[31] M. Cochet, G. Louarn, S. Quillard, J. P. Buisson, S. Lefrant, J. Raman Spectro., 31 (2000) 1041.

[32] X. Li, W, Chen, C. Bian, J. He, N. Xu, G. Xue, Appl. Surf. Sci., 217 (2003) 16.

[33] R. S. Mane, J. Chang, D. Ham, B. N. Pawar, T. Ganesh, B. W. Cho, J. K. Lee, S. H. Han, Curr. Appl. Phy., 9 (2009) 87.

[34] S. H. Mujawar, S. B. Ambade, T. Battumur, R. B. Ambade, S. H. Lee, Electrochim. Acta, 56 (2011) 4462.

[35] Z. Tong, Y. Yang, J. Wang, J. Zhao, B. L. Suc, Y. Li, J. Mater. Chem. A, 2 (2014) 4642.

[36] L. Wang, L. Chen, B. Yan, C. Wang, F. Zhu, X. Jiang, Y. Chao, G. Yang, J. Mater. Chem. A, 2 (2014) 8334.

[37] H. Guan, L. Z. Fan, H. Zhang, X. Qu, Electrochim. Acta, 56 (2010) 964.

[38] J. M. Ahn, A. I. Inamdar, Y. Jo, J. Kim, W. Jung, H. Im, H. S. Kim, J. Korean Phys. Soc., 64 (2014) L182.

[39] S.Richard Prabhu Gnanakan, N. Murugananthem, A. Subramania, Polym. Adva. Techn., 22 (2011) 788.

Figure Captions

Fig. 1: A) Schematic illustration and **B)** Actual experimental set up of chemical route for the deposition of PANI-TiO_2 composite thin films.

Fig. 2: A) Growth mechanism of the PANI-TiO_2 composite thin film formation and **B)** Photographs of the (a) PANI and (b) PANI-TiO_2 composite thin films on the stainless steel substrate.

Fig. 3: X-ray diffractograms of (a) PANI and (b) PANI-TiO_2 composite thin films on stainless steel substrate.

Fig. 4: The SEM micrographs of (a) PANI and (b) PANI-TiO_2 composite on stainless steel substrate at x 10,000 magnification.

Fig. 5: A) FT-IR and **B)** FT-Raman spectra of (a) PANI and (b) PANI-TiO_2 composite thin films.

Fig. 6: A) The CV curves of (a) PANI and (b) PANI-TiO_2 composite thin film electrodes at the scan rate of 5 mV/s; **B)** The CV curves of PANI-TiO_2 thin films at various scan rates. Variation of **C)** specific and **D)** interfacial capacitance as a function of scan rate of (a) PANI and (b) PANI-TiO_2 composite thin film electrodes in 1 M H_2SO_4 electrolyte.

Fig. **7:** The variation of specific capacitance with cycle number of (a) PANI and (b) PANI-TiO_2 composite thin film electrodes in 1 M H_2SO_4 electrolyte. Inset shows the CV curves of PANI-TiO_2 composite thin film electrode at 1^{st} and $5{,}000^{th}$ cycles.

Fig. 8: A) Galvanostatic charge-discharge curves; **B)** Nyquist plots of the (a) PANI and (b) PANI-TiO_2 composite thin film electrodes in 1 M H_2SO_4 electrolyte.

Figures

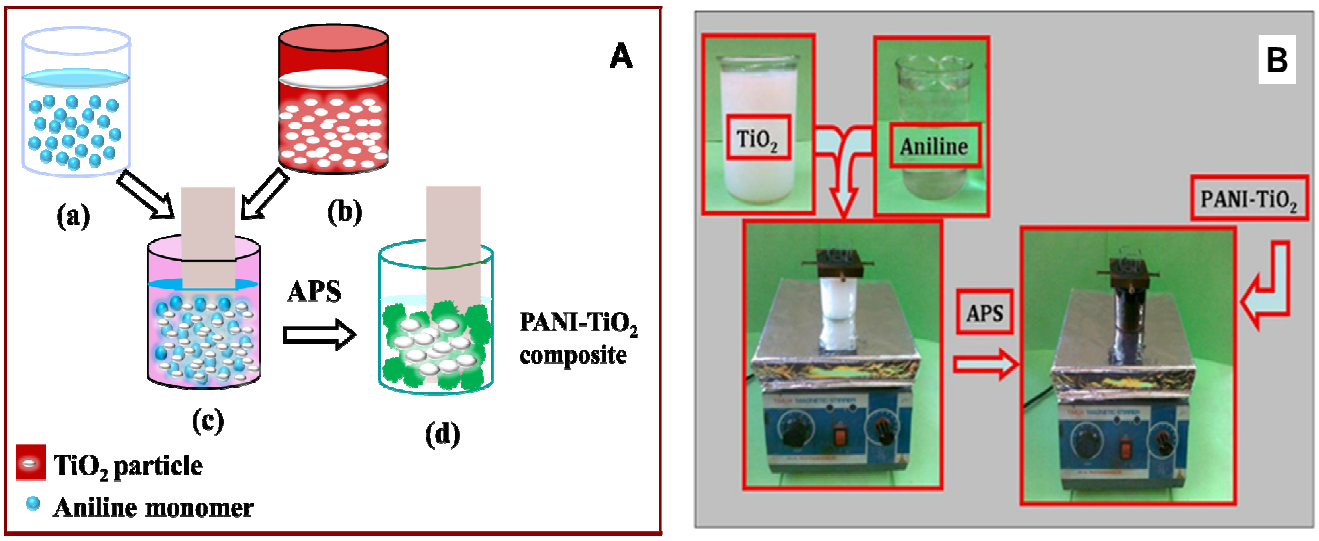

Fig. 1

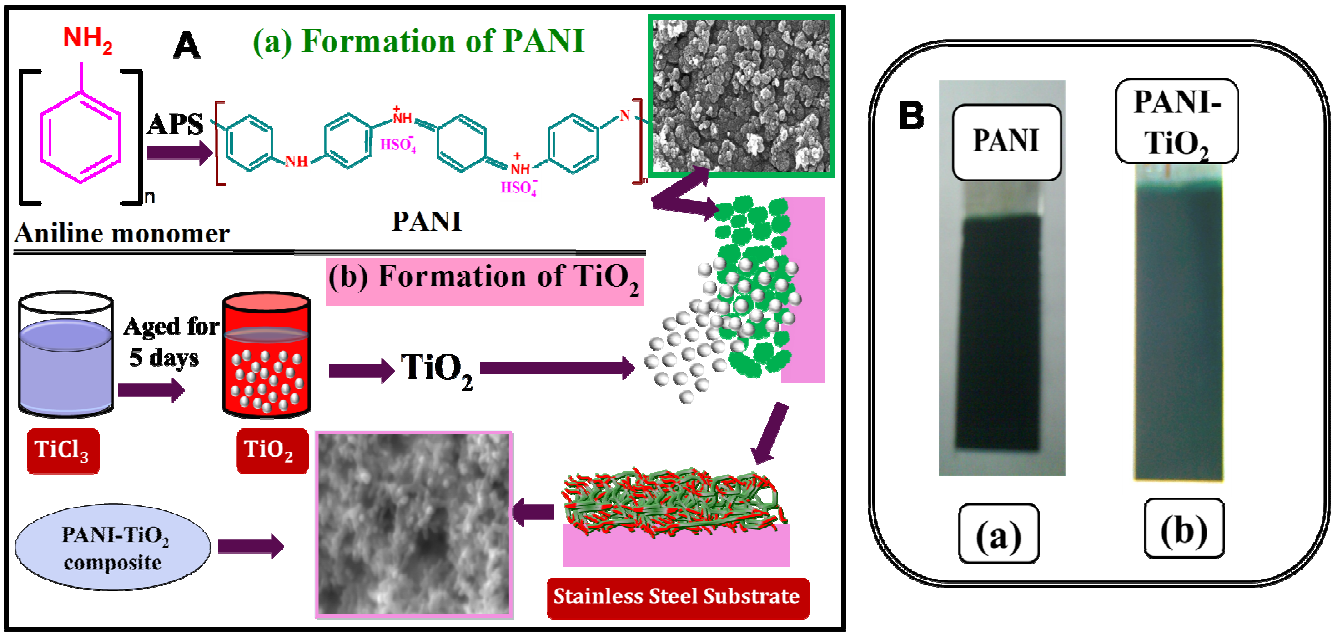

Fig. 2

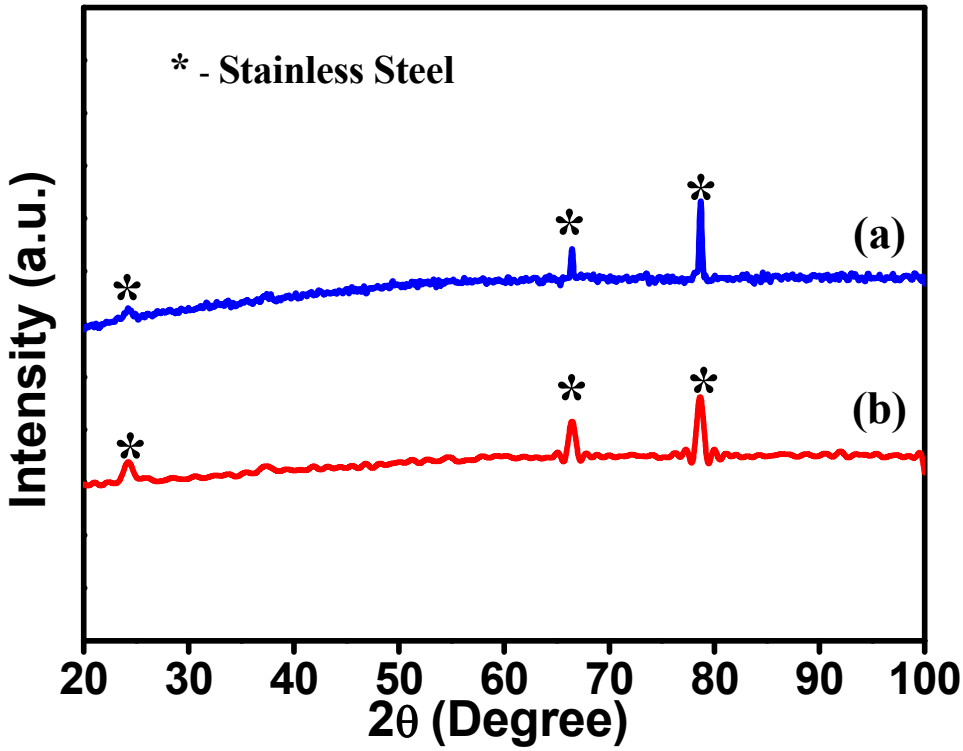
* - Stainless Steel
Intensity (a.u.)
(a)
(b)
20
30
40
50
60
70
80
90
100
2θ (Degree)

Fig. 3

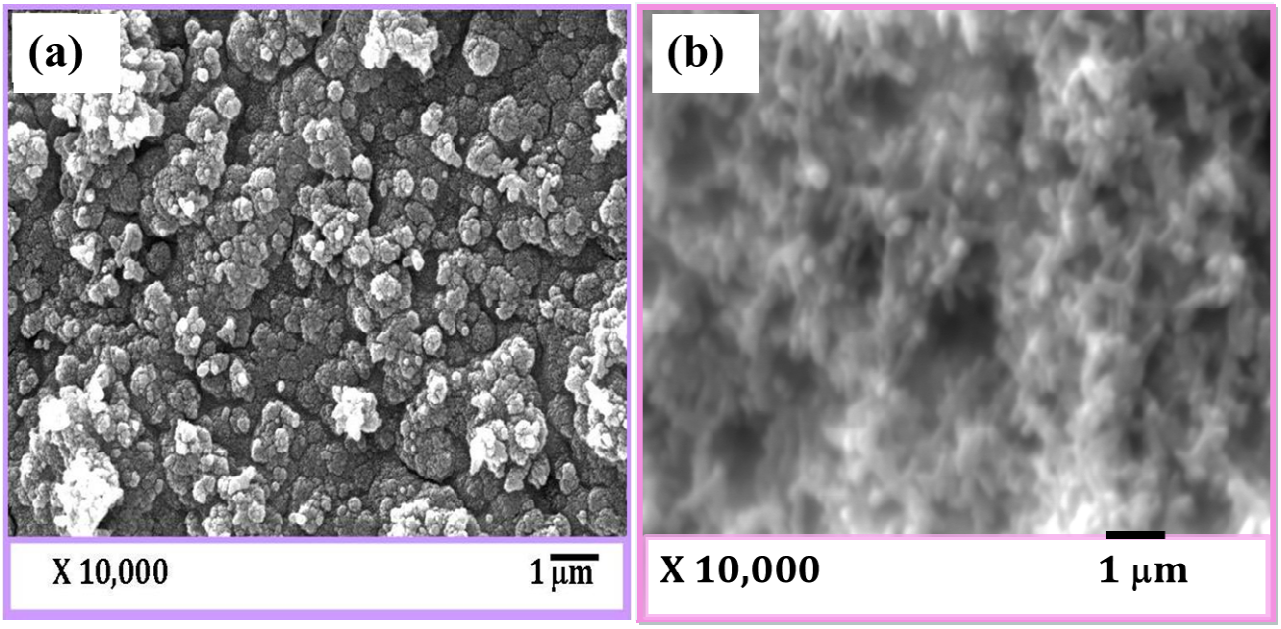
(a)
X 10,000
1 µm
(b)
X 10,000
1 µm

Fig. 4

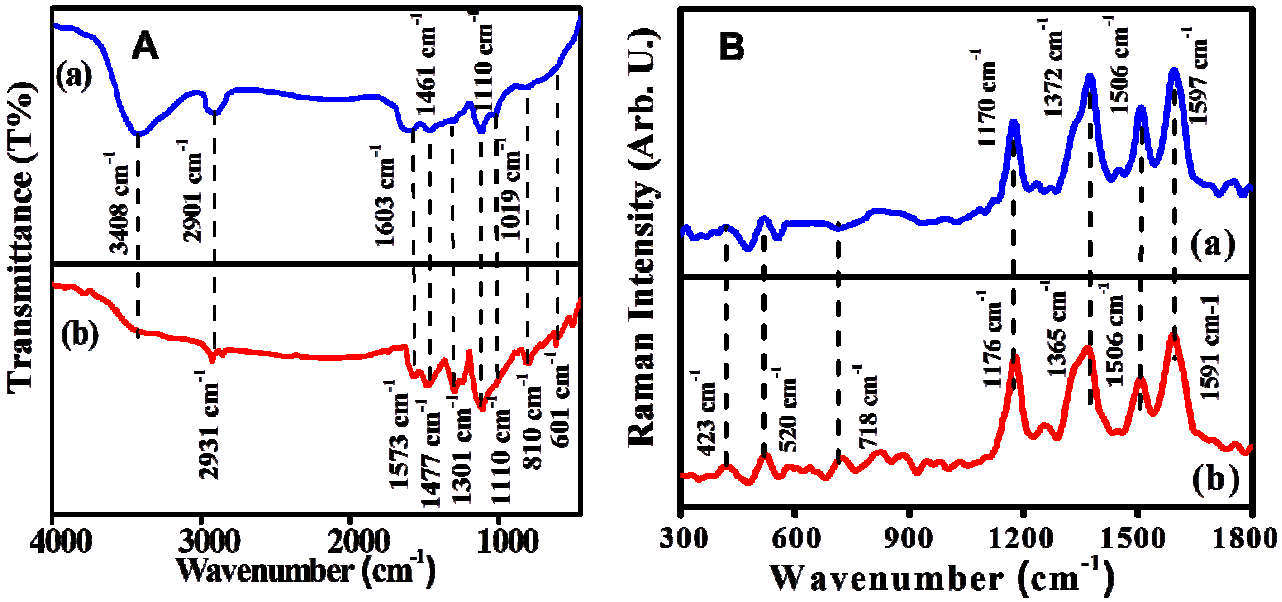
A
(a)
(b)
Transmittance (T%)
3408 cm-1
2901 cm-1
1603 cm-1
1461 cm-1
1110 cm-1
1019 cm-1
2931 cm-1
1573 cm-1
1477 cm-1
1301 cm-1
1110 cm-1
810 cm-1
601 cm-1
4000
3000
2000
1000
Wavenumber (cm-1)
B
Raman Intensity (Arb. U.)
1170 cm-1
1372 cm-1
1506 cm-1
1597 cm-1
423 cm-1
520 cm-1
718 cm-1
1176 cm-1
1365 cm-1
1506 cm-1
1591 cm-1
300
600
900
1200
1500
1800
Wavenumber (cm-1)

Fig. 5

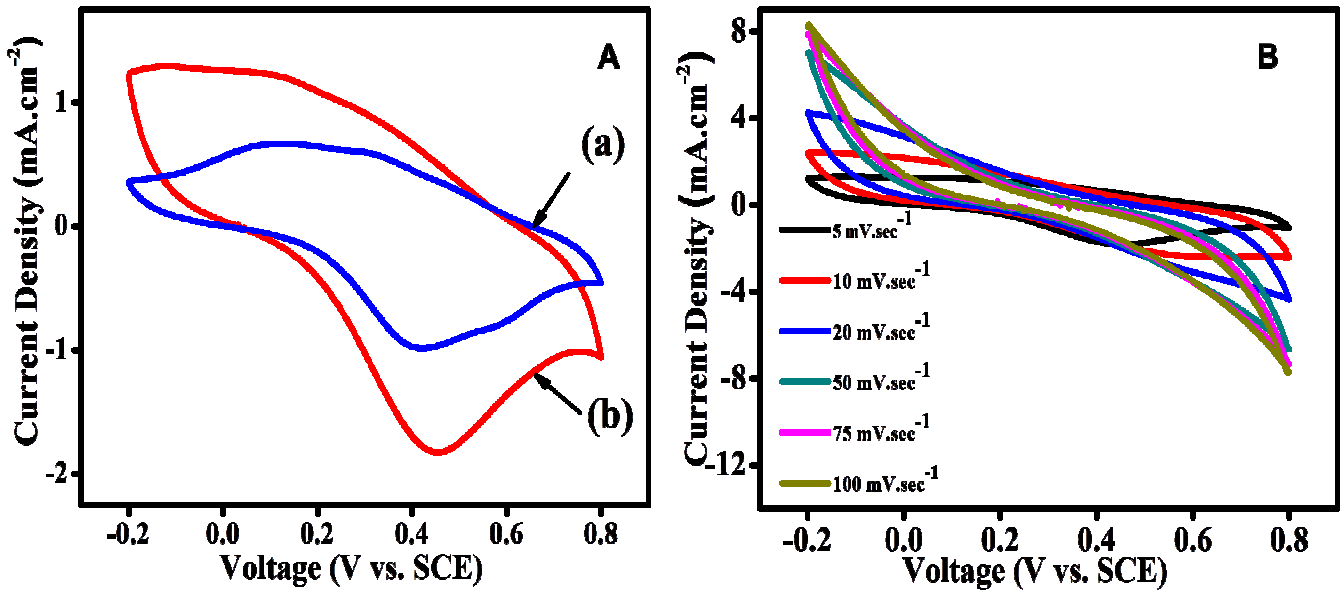
A
(a)
(b)
Current Density (mA.cm-2)
Voltage (V vs. SCE)
B
5 mV.sec-1
10 mV.sec-1
20 mV.sec-1
50 mV.sec-1
75 mV.sec-1
100 mV.sec-1
Current Density (mA.cm-2)
Voltage (V vs. SCE)

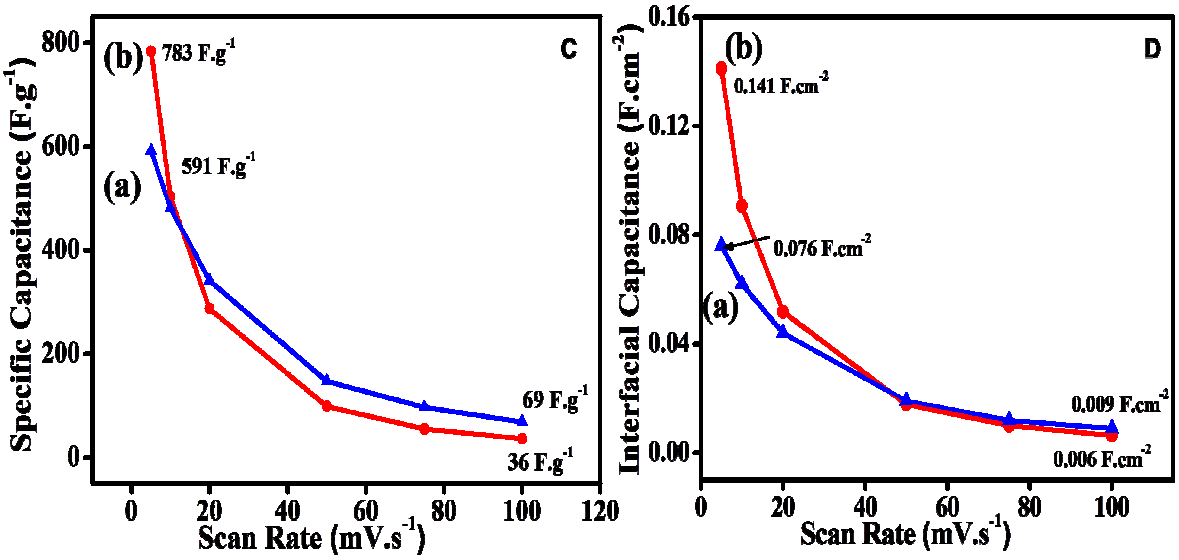
C
(b)
783 F.g-1
(a)
591 F.g-1
69 F.g-1
36 F.g-1
Specific Capacitance (F.g-1)
Scan Rate (mV.s-1)
D
(b)
0.141 F.cm-2
0.076 F.cm-2
(a)
0.009 F.cm-2
0.006 F.cm-2
Interfacial Capacitance (F.cm-2)
Scan Rate (mV.s-1)

Fig. 6

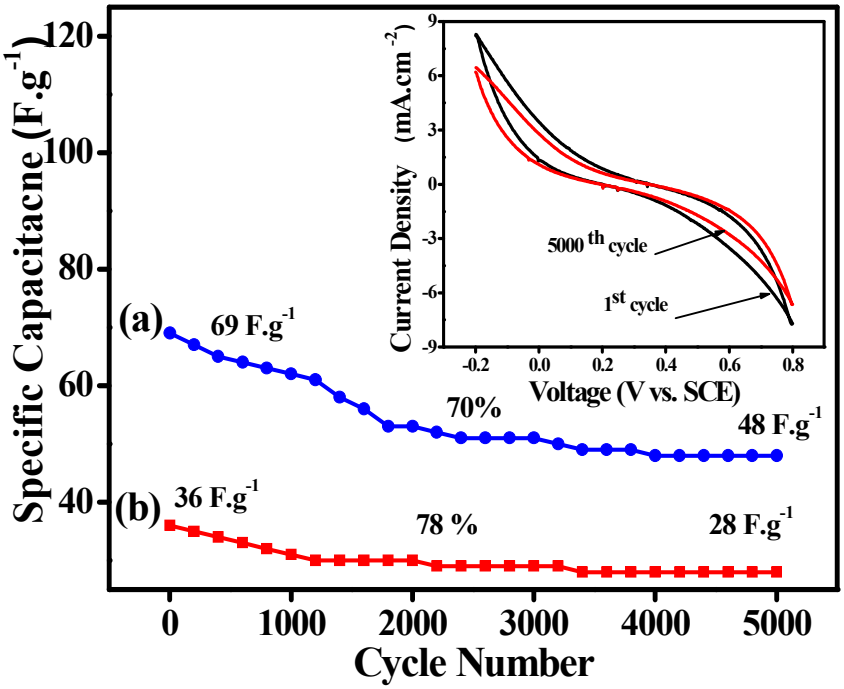
(a)
69 F.g-1
70%
48 F.g-1
(b)
36 F.g-1
78 %
28 F.g-1
Specific Capacitacne (F.g-1)
Cycle Number
Current Density (mA.cm-2)
5000 th cycle
1st cycle
Voltage (V vs. SCE)

Fig. 7

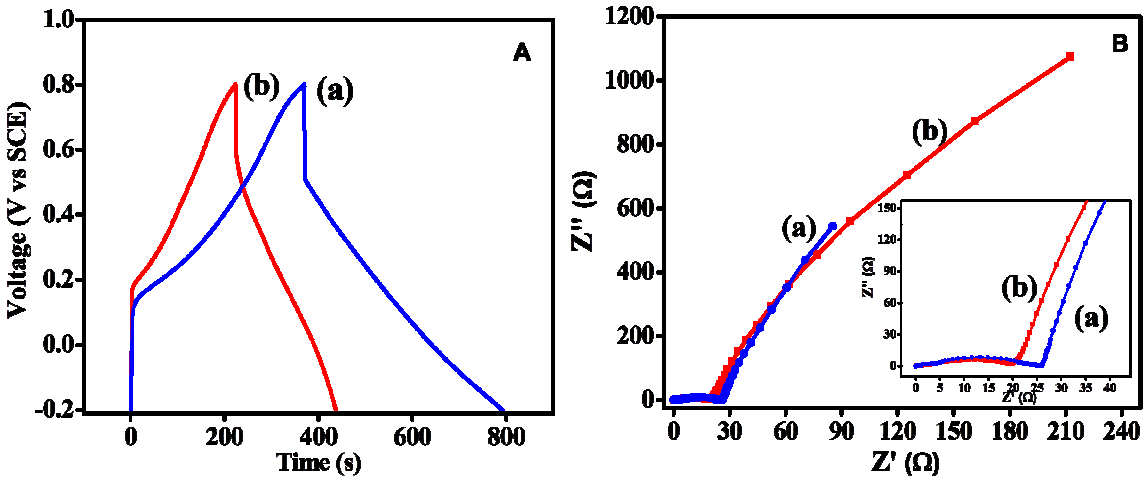
A
(b)
(a)
Voltage (V vs SCE)
Time (s)
1.0
0.8
0.6
0.4
0.2
0.0
-0.2
0
200
400
600
800
B
(b)
(a)
Z'' (Ω)
Z' (Ω)
1200
1000
800
600
400
200
0
0
30
60
90
120
150
180
210
240
(b)
(a)
Z'' (Ω)
Z' (Ω)
150
120
90
60
30
0
0
5
10
15
20
25
30
35
40

Fig. 8

Table 1: Summary of PANI–TiO_2 composite thin film based supercapacitor with their key performance features

Sr. No.	Material	Electrolyte	PW Volt	CD ($A.g^{-1}$)	Method	Cs $F.g^{-1}$	Ref.
1	PANI-APTES-TiO_2	1 M HCl	-0.2 to +1	0.5	Graft Polymerization of PANI on Self assembled monolayer (SAM) TiO_2 Nanotube Arrays	380	11
2	PANI/PNR/TiO_2	1 M H_2SO_4	-0.2 to +0.8	5 mA	Chemical Oxidative Polymerization Method	335	13
3	Polyaniline/TiO_2	1 M H_2SO_4	-0.2 to + 0.55	1.5	One-step in situ Oxidation Polymerization	330	14
4	PANI-TNT	1 M H_2SO_4	-0.2 to +1	3	Anodization (TNT) and Electrochemically polymerization (PANI)	740	31
5	PANI-TiO_2	1 M H_2SO_4	-0.2 to +0.8	2.7	Chemical Bath Deposition	709	CW

PW=Potential Window, CD= Current Density, Cs= Specific Capacitance, Ref = References, CW= Current Work

Table 2: Supercapacitive parameters of PANI and PANI-TiO_2 composite thin film electrodes

Parameters/ Material → ↓	PANI	PANI-TiO_2
Specific Energy (S.E.) $Wh.kg^{-1}$	295.5	391.5
Specific Power (S.P.) $kW.kg^{-1}$	0.70	1.83
Columbic Efficiency (η) %	87	96